# Optofluidic control using photothermal nanoparticles

GANG L. LIU[1,2], JAEYOUN KIM[1], YU LU[1] AND LUKE P. LEE[1,2]*

[1]Biomolecular Nanotechnology Center, Berkeley Sensor and Actuator Center, Department of Bioengineering, University of California at Berkeley, Berkeley, California 94720, USA
[2]UCSF and UCB Joint Graduate Group in Bioengineering, University of California, San Francisco, California 94143, USA
*e-mail: lplee@berkeley.edu

Published online: 18 December 2005; doi:10.1038/nmat1528

**Photothermal metallic nanoparticles have attracted significant attention owing to their energy-conversion properties[1–4]. Here, we introduce an optofluidic application based on a direct optical-to-hydrodynamic energy conversion using suspended photothermal nanoparticles near the liquid–air interface. Using light beams with submilliwatt power, we can drive and guide liquid flow in microfluidic channels to transport biomolecules and living cells at controlled speeds and directions. Previously, a variety of methods for controlling microscale liquid flow have been developed owing to the increasing interest for microfluidics-based biochemical analysis systems[5]. However, our method dispenses with the need for complex pump and valve devices[6–8], surface chemistry[9,10] and electrode patterning[11–14], or any other further effort towards substrate fabrication[15,16]. Instead, our optofluidic control method will allow the fabrication of all-optical large-scale integrated microfluidic circuits for biomolecular and cellular processing without any physical valve or mechanical pumping device.**

Here we use gold nanocrescent particles[17] (see Methods for the preparation details) with a strong absorption band around 780 nm (see Supplementary Information, Fig. S1) as the photothermal nanoparticles (PNPs). We believe that many other nanoparticles with potential photothermal properties such as Au nanoshells[3], nanorods[18], nanocages[19], nano-half-shells[20] as well as carbon nanotubes[21] can also be used as PNPs in optofluidic control. The PNP-activated optofluidic effect simultaneously involves evaporation, condensation, coalescence, contact-line pinning, surface wetting and many other phenomena within the millisecond timescale and micrometre dimension. This mechanism is fundamentally different from that of Marangoni flow[22,23] in which the liquid is driven by a surface-tension gradient. We propose that the mechanism of the PNP-activated optofluidic effect is as follows (Fig. 1a). At the beginning, the liquid on a hydrophobic surface remains stationary. The local concentration of PNPs near the liquid–air interface is higher than that of the interior owing to the 'coffee-ring' effect[24]. When a focused light illuminates the PNPs near the liquid–air interface, heat is generated and transferred from the PNPs to the surrounding liquid within tens of nanoseconds (see Supplementary Information), which significantly accelerates the liquid evaporation from the interface and produces vapour. In contrast, the original liquid contact line is pinned and liquid lost in evaporation is replenished from the interior region[24]. The vapour in the colder air condenses almost immediately after the evaporation and droplets form very close to or even in contact with the liquid–air interface. The droplets then coalesce with each other and grow into larger ones that eventually merge with the original liquid body and extend its contact line. Previous studies have shown that the droplet coalescence can facilitate flow significantly[25], and the surface wetting by the coalesced droplets also assists the advance of the liquid–air interface. The PNPs are drawn towards the new contact line because of the liquid motion and convection. The above processes can occur repeatedly and concurrently, and the liquid flow can be continuous if the light illumination is translated along with the advancing liquid–air interface.

In an experiment to support the proposed mechanism, a 2 μl water drop is dispensed on a hydrophobic glass slide (see Methods for the preparation details), and a focused 785 nm laser beam with tunable power is used as the illumination source. The contact angle of the water drop on the glass slide was approximately 60° (but this was not critical for our method). In the liquid we introduced ~1 nM PNPs. When a 20 mW, 785 nm focused light spot was illuminated on the liquid contact line and translated outwards, the liquid evaporation, droplet formation and contact-line advance are clearly visible (Fig. 1b). The optically controlled advance of the liquid–air interface follows the light translation and stops on the removal of the illumination (see Supplementary Information, Movie S1). However, as the liquid is unconfined in this case, the liquid flow cannot be guided unidirectionally and thus the flow speed is low.

In order to characterize the temperature distribution of the PNP-suspended liquid with a high spatial resolution, we measured the thermal fluorescence quenching[26] by fluorescence microscopy. As shown in Fig. 1c, a water solution containing 100 μM fluorescein, 1 M *N*-2-hydroxyethylpiperazine-*N*′-2′-ethanesulphonicacid (HEPES) buffer and 1 nM PNPs were illuminated by a 20 mW, 785 nm focused laser spot near the liquid–air interface for 1 s. The fluorescence intensity at the illuminated area decreased markedly owing to the localized increase in liquid temperature. The temperature distribution was then calculated according to the previously established relations between

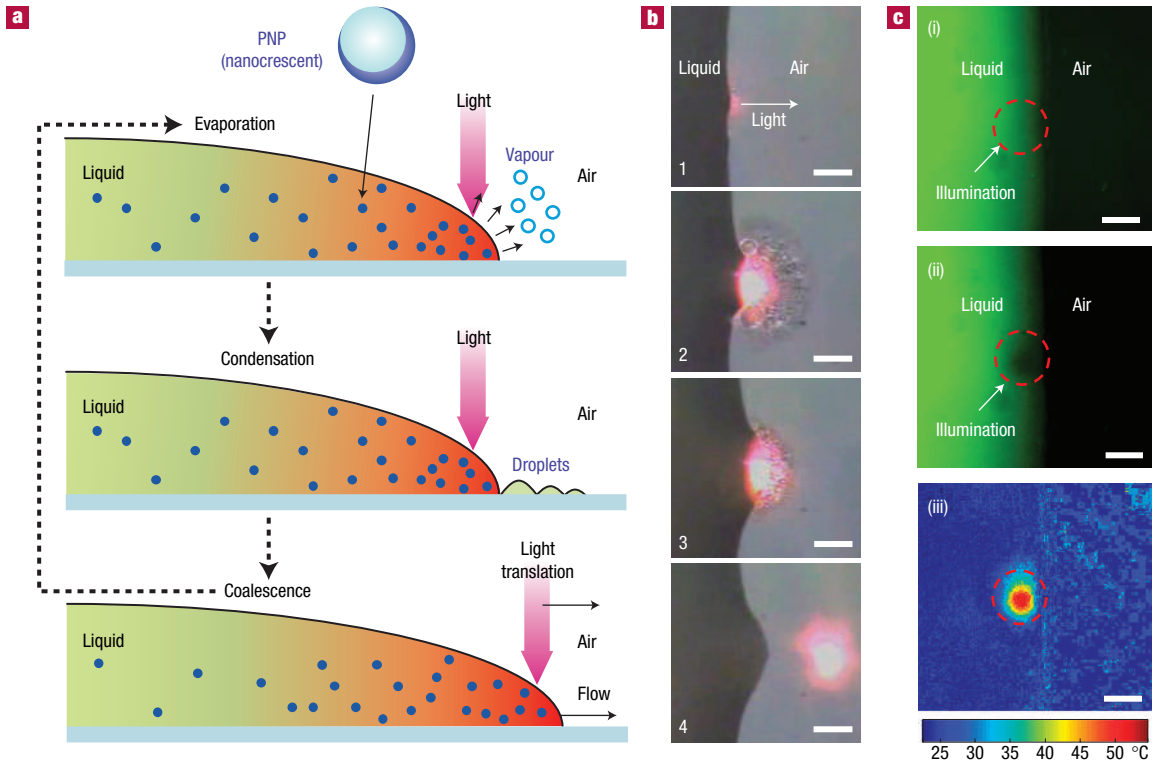


**Figure 1 PNP-activated optofluidic flow. a**, The principle of the optically controlled advance of the liquid–air interface. First, the focused light illumination on the PNPs increases the local temperature of the liquid and leads to water evaporation at the liquid–air interface. Second, the vapour in the relatively cold air condenses into droplets in front of the liquid–air interface. Third, the droplets coalesce with the original bulk liquid body and the liquid–air interface advances. The processes are repeated as the light is translated, so the optofluidic flow can be continuous. **b**, Video prints showing the light-driven advance of the liquid–air interface of a 1 nM PNP water solution on a glass surface. **c**, The temperature distribution in PNP-suspended liquid with the focused light illumination. The fluorescence images show a liquid containing 1 M HEPES, 100 μM fluorescein and 1 nM PNPs respectively (i) before and (ii) after 1-s focused illumination of 20 mW, 785 nm laser light on the area marked by the red circle. The colour-coded image in (iii) is the temperature distribution after the light illumination. All scale bars are 10 μm.

temperature and fluorescence intensity change (see Supplementary Information, Fig. S2). Most of the liquid body remains at room temperature (22 °C) except for the illuminated circular area with a ~10 μm diameter where the temperature shows a gaussian distribution and the highest temperature is close to 60 °C (lower than 100 °C owing to the energy loss in fluorescence thermal quenching). Another experiment using thermochromic microcapsules in the liquid also showed that the temperature of the liquid remains lower than 40 °C even at positions as close as 10 μm from the illuminated area where the water is boiling (see Supplementary Information, Fig. S3). Hence the optofluidic control method can be applied to transport liquid containing biomolecules and cells with their original integrities.

As polydimethylsiloxane (PDMS) microfluidic chips fabricated by soft lithography[27] have been extensively used in chemical, biomolecular and cellular analysis, we demonstrated the optofluidic control of PNP-suspended liquids in PDMS microfluidic chips. Unlike the unconfined flow of a millimetre-scale liquid drop shown above, the optically controlled fluidic flow in predefined microchannels is laminar and unidirectional. It shows a much higher flow speed as the vapour and droplets are bound within the channel and contribute to the liquid advance only along the channel direction and the minimized vertical convection in microchannels favours the heat concentration at the liquid–air interface. The microfluidic channels are formed by directly placing a PDMS slab (on which the water contact angle is 110°, see Supplementary Information, Fig. S4) with recessed grooves on the hydrophobic glass slide (Fig. 2a). Figure 2b shows that the 0.5 nM PNP-suspended 1X PBS buffer in a 40-μm-wide, 5-μm-high channel was driven and guided by the translation of a focused 10 mW, 785 nm laser spot at a speed of ~50 μm $s^{-1}$ (see Supplementary Information, Movie S2). The liquid remains stationary in the hydrophobic channel without the light guide owing to the balanced surface energy, and no thermocapillary flow is seen when the light spot illuminates the interior of the liquid. The liquid flow stops immediately after the light translation stops, and liquid motion in the microchannel is under complete control without any valve or pump. For a channel width (80 μm) much larger than the focused light spot (10 μm), the optofluidic flow can also be realized (see Supplementary Information, Movie S2). An extruding liquid flow is generated as only a portion of the liquid–air interface is illuminated by the light spot (Fig. 2c).

With PNPs, the liquid flow in parallel 10-μm-wide microfluidic channels can be driven and guided simultaneously by a focused laser line at the speed of ~10 μm $s^{-1}$ as shown in Fig. 2d (see Supplementary Information, Movie S3). It is worth noting that the light power illuminated on each channel is smaller than 1 mW. Pure water and 60-nm gold colloidal nanoparticles with an absorption band unmatched to the laser wavelength were introduced as the controls (Fig. 2e) in two parallel channels. They show no water evaporation, no droplet formation and thus no response to the optofluidic control. As a side-by-side comparison,

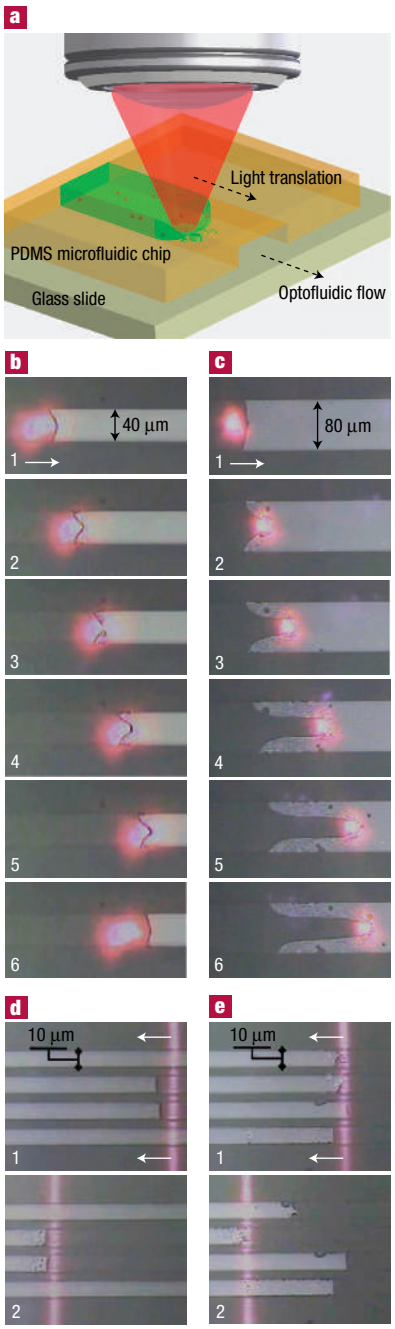


**Figure 2 Optofluidic control in straight microfluidic channels. a**, Illustration of the experimental system configuration. **b**, Optofluidic control in a 40-μm-wide channel. The video prints show that the flow of the 0.5 nM PNP-suspended 1X PBS buffer solution follows the optical guiding of a 10 mW, 785 nm laser spot at a speed of ~50 μm $s^{-1}$ (frames 1–5) and stops otherwise (frame 6). **c**, Optofluidic control in an 80-μm-wide channel. The 1 nM PNP water solution is guided by a 10 mW, 785 nm laser spot at a speed of ~50 μm $s^{-1}$. **d**, Simultaneous optofluidic controls of 1 nM PNP water solutions in two parallel 10-μm-wide channels by a focused laser line with sub-milliwatt illumination power on each channel. Other channels are intentionally left empty for better image contrast. Frames 1 and 2 show the channels respectively before and after the light translation at a speed of ~10 μm $s^{-1}$. **e**, Optofluidic control of four different liquids. From top to bottom, 0.2 nM and 1 nM PNP water solution, pure deionized water and 60-nm Au colloidal nanospheres are introduced into the 10-μm-wide channels, respectively. Frames 1 and 2 show the channels respectively before and after the light translation at a speed of ~10 μm $s^{-1}$.

PNP-activated optofluidic flows in the adjacent two parallel channels were observed. The maximal optofluidic flow speeds in these two channels are different because the introduced liquids have different PNP concentrations.

Among the involved physical mechanisms, we believe that the rate of droplet formation, growth and coalescence limits the overall optofluidic flow speed to ~1 mm $s^{-1}$ (see the calculation details provided in Supplementary Information). As the light illumination power, microchannel dimension and PNP concentration are three major tunable factors to determine the rate of droplet formation and coalescence, we characterized the optofluidic flow speed accordingly. Figure 3a shows the maximal speed of the optofluidic flow versus the power of light illumination for 1 nM PNP solutions and Fig. 3b shows the maximal flow speed versus the PNP concentration for 20-mW illumination power. The characterizations were carried out for three different channel widths: 10, 40 and 80 μm. We found that the maximal optofluidic flow speed in the 10 μm channel can be as high as 500 μm $s^{-1}$ using the 20 mW light power. The flow speed can be further increased by adopting narrower microchannels, more accurate light control and PNPs with higher photothermal efficiency.

In addition to individual straight channels, a functional microfluidic circuit often consists of channel junctions. The positioning of liquid flow at channel junctions requires complicated valve systems[7]. Here we demonstrate the optofluidic control with superior directionality at the channel junctions without any valve or pump. In the two adjacent T-shaped junctions, 1 nM PNP water solution is introduced from the right branch channel (Fig. 4a). All channels with the same width (40 μm) are open to the atmosphere and no previous surface patterning was performed; all the channels therefore have an equal chance to be filled with pressure-driven flow. The video prints show the PNP-activated optofluidic flow controlled by a 20 mW, 785 nm laser spot through the two junctions with an emphasis on two sharp turns (see Supplementary Information, Movie S4). In three experimental trials, the liquid was optically driven and guided into three different branches without filling other branches as shown in Fig. 4b. The optofluidic flow speed remains almost the same after the liquid enters the chosen branch, even with sharp turns, because most of the PNPs near the liquid–air interface will follow the direction of the guiding light and be drawn to the advancing liquid–air interface. Among the channel junction structures, the mixer is one of the most common components in microfluidic biochips. Here, we demonstrate that the liquids in three respective channels can be mixed with optofluidic control as shown in Fig. 4c (see Supplementary Information, Movie S5). The optofluidic flow speed becomes much faster after the liquid mixing, which indicates that the PNPs in the three fluids mix together and become concentrated. We believe that the PNP-activated optofluidic control can be realized in a microfluidic 'maze' with many junctions in various shapes.

Not only can soluble molecules be transported in microfluidic devices with optofluidic control, but living cells can also be transported. In order to test the cell viability when co-cultured with PNPs, three types of cell, Jurkat T-cells, Chinese hamster ovary cells and HeLa cells, were stained with Calcein AM green fluorescent dye. We found that the gold-based PNPs have negligible toxicity to these three cell lines after an incubation of 24 h, and the cells can still proliferate (not shown). The gold-based nanoparticles have been proved for a long time to be compatible with many cell lines, and have been used for intracellular molecular sensing and delivery. The optofluidic transportation of single and multiple Jurkat T-cells with PNP-suspended culture media in 100-μm-wide, 50-μm-high PDMS channels is demonstrated (see Supplementary Information, Fig. S5 and Movie S6). Most of the cells can be transported intact (no fluorescence intensity decrease), even including those that are

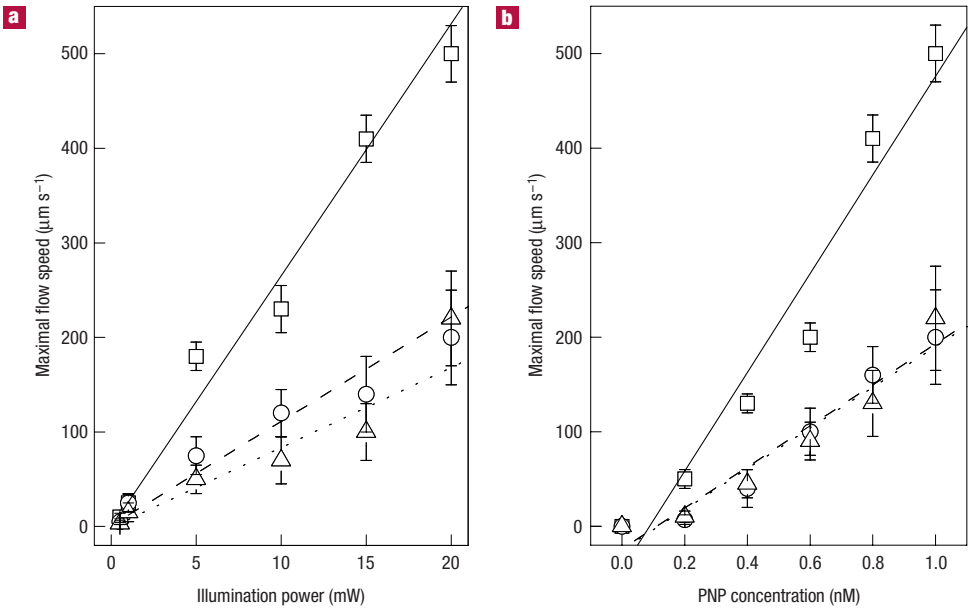


**Figure 3 Maximal flow speed by optofluidic control. a**, Maximal flow speed of the 1 nM PNP water solution versus the illumination optical power. The open square, circle and triangle correspond to the microchannels with widths of 10, 40 and 80 μm, respectively. The solid, dashed and dotted lines represent the linear fits of the above three data sets, respectively. **b**, Maximal flow speed versus the PNP concentration for the optofluidic control with a 20 mW laser spot. The symbols and lines have the same representations as those in **a**. The error bars in both plots represent the standard deviation of the five measurements for each data point.

only several micrometres away from the laser spot. Some of cells can adhere to the surface and they are alive after the attachment. The other two types of cell, Chinese hamster ovary cells and HeLa cells, were also tested and can be transported in the similar fashion.

We believe that optofluidic control using PNPs in nano- or microfluidic circuits allows the creation of a large-scale all-optical biofluidic microprocessor for biomolecular and cellular medicine. With the assistance of laser beam scanning or spatial light modulation apparatus, automated and multiplexed optofluidic controls with high precision can be realized. The complexity and cost of the microfluidic biochips can be greatly reduced using complete optofluidic control. In addition to applications in biochips, the optohydrodynamic energy-conversion scheme using metallic nanoparticles also has implicational importance to nano- and microscale water power systems, solar heating systems and other optically powered nanomachines in aqueous environments.

## METHODS

### PREPARATION OF PNPS

The PNPs, gold nanocrescents, were prepared by the following method[17]. First, 100-nm polystyrene nanoparticles (Duke Scientific, California) were dispersed on a silicon wafer with a thin film of chromium coating; second, a thin layer (15–20 nm) of gold was deposited on the polystyrene nanoparticles from an oblique angle (~60° with respect to the wafer surface) when the wafer was rotating at a speed of 60 r.p.m.; third, the polystyrene nanoparticles with gold nanocrescent shell were lifted off from the wafer by sonication and collected in water suspensions; finally, the PNP suspension was subjected to 300 r.p.m. centrifugation for a few minutes and 0.4-μm nanopore filtering to remove impurities. The PNP concentration can be controlled by the number of polystyrene nanoparticles (concentration provided by the vendor) dispersed on the wafer and the final suspension volume. We made ~1 nM, or $\sim 10^{14}$ particles $l^{-1}$, PNP suspension as our stock solution.

### CALIBRATION OF TEMPERATURE VERSUS FLUORESCENCE INTENSITY

The decrease of thermally induced fluorescence intensity versus increase of temperature was characterized by heating the liquid containing 100 μM fluorescein, 1 M HEPES buffer and 1 nM photothermal nanoparticles using an electric resistor heater and measuring the temperature with a thermal couple. The liquid was enclosed in a millimetre-scale transparent chamber to minimize evaporation during the heating, because water evaporation causes an increase of the fluorophore concentration and fluorescence intensity. The liquid was heated from room temperature (22 °C) to ~70 °C, and the fluorescence intensity decreased (see Supplementary Information, Fig. S2). The mercury-lamp illumination was turned on only when the fluorescence images were being taken, which minimized the effect of photobleaching in our measurements. When the temperature was higher than 70 °C, the water evaporated very rapidly and the measurements were no longer accurate.

### THERMOCHROMIC MICROCAPSULE TEMPERATURE INDICATOR

Three kinds of thermochromic microcapsule were kindly provided by Kelly Chemical (Taiwan). The light-yellow, magenta and dark-blue microcapsules became colourless when the temperature was higher than 30, 40 and 70 °C, respectively. We mixed them together in water and in 1 nM PNP suspension, respectively. For the sample of thermochromic microcapsules in water, we used an electric resistor heater to increase its temperature and a thermal couple to measure the temperature (see Supplementary Information, Fig. S3a,b). Owing to the low colour contrast of the light-yellow microcapsules, their colour change was unclear. The magenta microcapsules become colourless when the temperature rose to 40 °C, whereas the dark-blue microcapsules remained the same colour as expected. For the sample of thermochromic microcapsules in PNP suspension, we used a 10 mW, 785 nm focused laser spot to illuminate the liquid–air interface. We observed that nearly all the magenta and dark-blue thermochromic microcapsules remained the same colour while water was boiling at the liquid–air interface, even when they were only a few micrometres away from the laser spot (see Supplementary Information, Fig. S3c,d).

### PREPARATION OF HYDROPHOBIC GLASS SLIDES AND PDMS MICROFLUIDIC CHIPS

The hydrophobic glass slides were prepared in the following way. Precleaned 1-mm-thick glass slides (Fisher Scientific, Pennsylvania) were incubated in a hexamethyldisilazane vapour deposition chamber for 10 min to form a hydrophobic hexamethyldisilazane monolayer on the glass surface. The glass slides were also subject to acetone and isopropanol wash to remove dust before immediate use. The PDMS microfluidic chip was made by the following procedure: first, a replication mould consisting of 5-μm-high ridges was photolithographically patterned on a silicon wafer using SU-8 2005

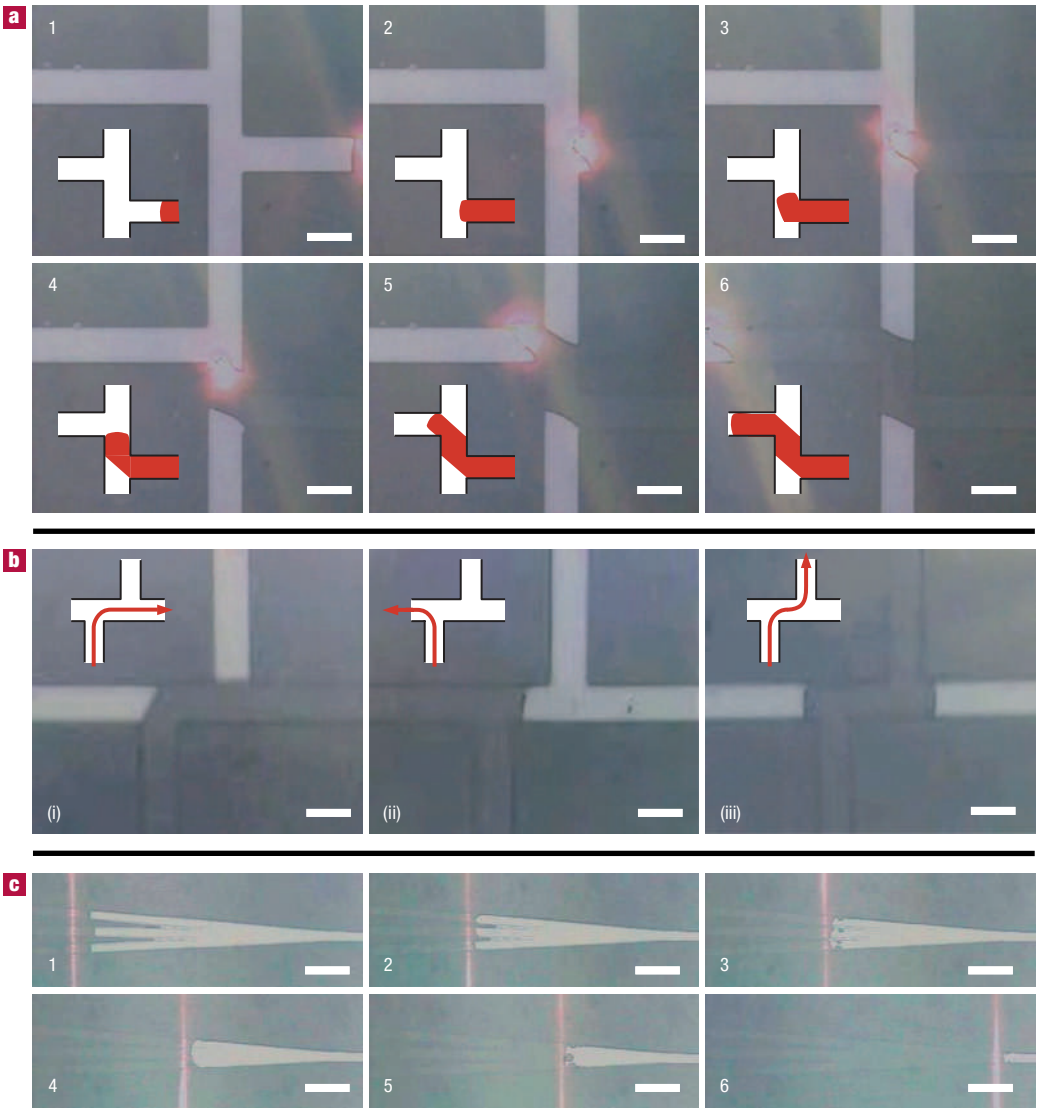


**Figure 4 Optofluidic control at two adjacent T-shaped channel junctions. a**, Video prints showing that a 1 nM PNP water solution introduced from the right channel is optically guided into the left channel after two sharp turns without filling the other two channels. **b**, Optofluidic control of liquid flow into three distinct paths at the two junctions without filling undesired channels. **c**, Optofluidic mixing of three separate liquid streams into one. All scale bars are 50 μm.

negative-tone photoresist (MicroChem, Massachusetts); second, the 10:1 mixture of PDMS monomer and curing agent (Dow Corning) was cast on the SU-8 mould to become a 500-μm-thick film, which was cured in an oven at 90 °C for 10 min; after the PDMS film was completely solidified, it was peeled off from the mould and recessed grooves in the same pattern as the mould generated on the PDMS surface. PDMS slabs with groove patterns were cut from the film using a razor blade, and these were then directly placed on the hydrophobic glass to form the microfluidic devices that we used in our experiments. As a microchannel is an enclosed structure and it is difficult to measure the liquid contact angles inside, as an alternative we measured the contact angles of a water droplet sandwiched by a PDMS slab and a hydrophobic glass slide (see Supplementary Information, Fig. S4). We then used a measurement system for liquid contact angles (Kruss USA, California) to acquire the side-view image and calculate the contact angles.

Received 18 July 2005; accepted 11 October 2005; published 18 December 2005.

## References

1. Boyer, D., Tamarat, P., Maali, A., Lounis, B. & Orrit, M. Photothermal imaging of nanometer-sized metal particles among scatterers. *Science* **297,** 1160–1163 (2002).
2. Cognet, L. *et al.* Single metallic nanoparticle imaging for protein detection in cells. *Proc. Natl Acad. Sci. USA* **100,** 11350–11355 (2003).
3. Kato, H., Nishizaka, T., Iga, T., Kazuhiko, K. Jr & Ishiwata, S. Imaging of thermal activation of actomyosin motors. *Proc. Natl Acad. Sci. USA* **96,** 9602–9606 (1999).
4. Sershen, S. R., Westcott, S. L., Halas, N. J. & West, J. L. Independent optically addressable nanoparticle-polymer optomechanical composites. *Appl. Phys. Lett.* **80,** 4609–4611 (2002).
5. Meldrum, D. R. & Holl, M. R. Microscale bioanalytical systems. *Science* **297,** 1197–1198 (2002).
6. Ho, C. H. & Tai, Y. C. Micro-electro-mechanical-systems (MEMS) and fluid flows. *Annu. Rev. Fluid Mech.* **30,** 579–612 (1998).
7. Unger, M. A., Chou, H. P., Thorsen, T., Scherer, A. & Quake, S. R. Monolithic microfabricated valves and pumps by multilayer soft lithography. *Science* **288,** 113–116 (2002).
8. Neale, S. L., Macdonald, M. P., Dholakia, K. & Krauss, T. F. All-optical control of microfluidic components using form birefringence. *Nature Mater.* **4,** 530–533 (2005).
9. Chaudhury, M. K. & Whitesides, G. M. How to make water run uphill. *Science* **256,** 1539–1541 (1992).
10. Kataoka, D. E. & Troian, S. M. Patterning liquid flow on the microscopic scale. *Nature* **402,** 794–797 (1999).
11. Harrison, D. J. *et al.* Micromachining a miniaturized capillary electrophoresis-based chemical analysis system on a chip. *Science* **261,** 895–897 (1993).
12. Burns, M. A. *et al.* Microfabricated structures for integrated DNA analysis. *Proc. Natl Acad. Sci. USA* **93,** 5556–5561 (1996).
13. Gallardo, B. S. *et al.* Electrochemical principles for active control of liquids on submillimeter scales. *Science* **283,** 57–60 (1999).
14. Lee, J., Moon, H., Fowler, J., Schoellhammer, T. & Kim, C.-J. Electrowetting and electrowetting-on-dielectric for microscale liquid handling. *Sensors Actuators A* **95,** 259–268 (2002).
15. Ichimura, K., Oh, S.-K. & Nakagawa, M. Light-driven motion of liquids on a photoresponsive surface. *Science* **288,** 1624–1626 (2000).

16. Chiou, P. Y., Moon, H., Toshiyoshi, H., Kim, C.-J. & Wu, M. C. Light actuation of liquid by optoelectrowetting. *Sensors Acutators A* **104,** 222–228 (2003).
17. Lu, Y., Liu, G. L., Kim, J., Mejia, Y. X. & Lee, L. P. Nanophotonic crescent moon structures with sharp edge for ultrasensitive biomolecular detection by local electromagnetic field enhancement effect. *Nano Lett.* **5,** 119–124 (2005).
18. Chou, C.-H., Chen, C.-D. & Wang, C. R. C. Highly efficient, wavelength-tunable, gold nanoparticle based optothermal nanoconvertors. *J. Phys. Chem. B* **109,** 11135–11138 (2005).
19. Chen, J. *et al.* Gold nanocages: Engineering the structure for biomedical applications. *Adv. Mater.* **17,** 2255–2261 (2005).
20. Love, J. C., Gates, B. D., Wolfe, D. B., Paul, K. E. & Whitesides, G. M. Fabrication and wetting properties of metallic half-shells with submicron diameters. *Nano Lett.* **2,** 891–894 (2002).
21. Kam, N. W. S., O'Connell, M., Wisdom, J. A. & Dai, H. Carbon nanotubes as multifunctional biological transporters and near-infrared agents for selective cancer cell destruction. *Proc. Natl Acad. Sci. USA* **102,** 11600–11605 (2005).
22. Edwards, D., Brenner, H. & Wasan, D. *Interfacial Transport Processes and Rheology* (Bufferworth-Heinemann, Boston, 1991).
23. Farahi, R. H., Passian, A., Ferrell, T. L. & Thundat, T. Marangoni forces created by surface plasmon decay. *Opt. Lett.* **30,** 616–618 (2005).
24. Deegan, R. D. *et al.* Capillary flow as the cause of ring stains from dried liquid drops. *Nature* **389,** 827–829 (1997).
25. Daniel, S., Chaudhury, M. K. & Chen, J. C. Fast drop movements resulting from the phase change on a gradient surface. *Science* **291,** 633–636 (2001).
26. Croonen, Y. *et al.* Influence of salt, detergent concentration, and temperature on the fluorescence quenching of 1-methylpyrene in sodium dodecyl-sulfate with meta-dicyanobenzene. *J. Phys. Chem.* **87,** 1426–1431 (1983).
27. Xia, Y. N. & Whitesides, G. M. Soft lithography. *Angew. Chem. Int. Edn Engl.* **37,** 551–575 (1998).

## Acknowledgements

The authors gratefully acknowledge financial support from the Defense Science Office of the Defense Advanced Research Projects Agency, USA. J.K. was supported by a grant (05K1501-02810) from the Center for Nanostructured Materials Technology under the 21st Century Frontier R&D Programs of the Ministry of Science and Technology, Korea.
Correspondence and requests for materials should be addressed to L.P.L.
Supplementary Information accompanies this paper on www.nature.com/naturematerials.

## Competing financial interests

The authors declare that they have no competing financial interests.